THE JOURNAL OF BIOLOGICAL CHEMISTRY
Vol. 279, No. 51, Issue of December 17, pp. 52840–52849, 2004

Printed in U.S.A.

EPR Spectroscopic Characterization of the Manganese Center and a Free Radical in the Oxalate Decarboxylase Reaction

IDENTIFICATION OF A TYROSYL RADICAL DURING TURNOVER*[S]

Received for publication, March 2, 2004, and in revised form, August 23, 2004
Published, JBC Papers in Press, October 7, 2004, DOI 10.1074/jbc.M402345200

Christopher H. Chang‡§, Draženka Svedružić‡, Andrzej Ozarowski‡¶, Lee Walker‡‖, Gregory Yeagle, R. David Britt**, Alexander Angerhofer‡, and Nigel G. J. Richards‡ ‡‡**

*From the ‡Department of Chemistry, University of Florida, Gainesville, Florida 32611-7200 and the **Department of Chemistry, University of California at Davis, Davis, California 95616*

Several molecular mechanisms for cleavage of the oxalate carbon-carbon bond by manganese-dependent oxalate decarboxylase have recently been proposed involving high oxidation states of manganese. We have examined the oxalate decarboxylase from *Bacillus subtilis* by electron paramagnetic resonance in perpendicular and parallel polarization configurations to test for the presence of such species in the resting state and during enzymatic turnover. Simulation and the position of the half-field Mn(II) line suggest a nearly octahedral metal geometry in the resting state. No spectroscopic signature for Mn(III) or Mn(IV) is seen in parallel mode EPR for samples frozen during turnover, consistent either with a large zero-field splitting in the oxidized metal center or undetectable levels of these putative high-valent intermediates in the steady state. A narrow, featureless $g = 2.0$ species was also observed in perpendicular mode in the presence of substrate, enzyme, and dioxygen. Additional splittings in the signal envelope became apparent when spectra were taken at higher temperatures. Isotopic editing resulted in an altered line shape only when tyrosine residues of the enzyme were specifically deuterated. Spectral processing confirmed multiple splittings with isotopically neutral enzyme that collapsed to a single prominent splitting in the deuterated enzyme. These results are consistent with formation of an enzyme-based tyrosyl radical upon oxalate exposure. Modestly enhanced relaxation relative to abiological tyrosyl radicals was observed, but site-directed mutagenesis indicated that conserved tyrosine residues in the active site do not host the unpaired spin. Potential roles for manganese and a peripheral tyrosyl radical during steady-state turnover are discussed.

The oxalate decarboxylase (OxDC,[1] or YvrK based on the corresponding open reading frame) from *Bacillus subtilis* has recently garnered attention because of its mechanistically intriguing reaction (1–4) (Scheme 1). Purified OxDC crystallizes as a hexamer of 43-kDa subunits, each of which is a member of the "bicupin" structural family (5), and contains two mononuclear manganese centers with amino acid ligands that are functionally similar to those of manganese superoxide dismutase (MnSOD) (6); namely three histidine residues and one carboxylic acid residue. Oxalate ^{13}C and ^{18}O isotope effects on V_{max}/K_m of YvrK suggest the presence of a slow, partially rate-determining step prior to the irreversible C-C bond cleavage (4), which was proposed to be a proton-coupled electron transfer.

The requirement for and substoichiometric consumption of dioxygen in the YvrK catalytic process, involvement of open shell manganese (2), and chemical precedent for oxalate decarboxylation in the Kolbe electrolysis (7, 8) and the Borodin-Hunsdiecker reaction (9–11) have led to various mechanistic proposals involving radical intermediates, and enzymic manganese complexes with formal oxidation states of either Mn(III) (2, 4) or Mn(IV) (3). A previously published electron paramagnetic resonance (EPR) spectrum of the enzyme in the resting state confirmed the presence of Mn(II) but did not address the question of higher valence states under turnover conditions (2).

The current work addresses the valence of the manganese center that predominates in the resting state and after oxalate addition with perpendicular and parallel mode electron paramagnetic resonance spectroscopy. In addition, the identity of an observed radical species appearing shortly after oxalate addition was established using isotopically edited oxalate, O_2, solvent, and protein. The time course of radical production and decay was estimated by kinetic simulation using a simple model, and compared with the overall rate of enzyme turnover. Finally, the power saturation and temperature response of the radical species were explored, and line shape features compared with known enzymatic species in order to propose an identity for the observed species.

EXPERIMENTAL PROCEDURES

Materials—Potassium oxalate, oxalic acid, and Amicon ultrafiltration membranes were obtained from Fisher. d_4-L-Tyrosine, the Proteo-Profile Trypsin In-Gel Digest Kit, *N,N*-bis(2-hydroxyethyl)-2-aminoethanesulfonic acid (BES), and piperazine were from Sigma-Aldrich. The

* This work was supported by National Institutes of Health (NIH) Grant NRSA DK61193 (to C. H. C.), NIH Grant DK61666 (to A. O., N. G. J. R.) National Science Foundation (NSF) CHE79008 (to N. G. J. R.), NSF MCB9983034 (to L. W. and A. A.), and NSF MCB9874541 and NIH GM48242 (to G. Y. and R. D. B.). The costs of publication of this article were defrayed in part by the payment of page charges. This article must therefore be hereby marked "*advertisement*" in accordance with 18 U.S.C. Section 1734 solely to indicate this fact.

[S] The on-line version of this article (available at http://www.jbc.org) contains Supplemental Material.

§ To whom correspondence may be addressed. Fax: 352-846-2095; E-mail: cchang@chem.ufl.edu.

¶ Current address: B120 NHMFL FSU, 1800 E. Paul Dirac Dr., Tallahassee, FL 32310-3706.

‖ Current address: Dept. of Biochemistry, University of California at Riverside, Riverside, CA 92521.

‡‡ To whom correspondence may be addressed. E-mail: richards@qtp.ufl.edu.

[1] The abbreviations used are: OxDC, oxalate decarboxylase; BES, *N,N*-bis(2-hydroxyethyl)-2-aminoethanesulfonic acid buffer; DPPH, 1,1-diphenyl-2-picrylhydrazyl; EPR, electron paramagnetic resonance; G, Gauss; MnSOD, manganese-dependent superoxide dismutase; ZFS, zero-field splitting; M.A., modulation amplitude.

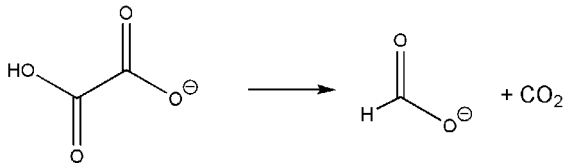

SCHEME 1. **The overall reaction catalyzed by YvrK is shown.**

sodium salt of [^{13}C]oxalic acid was obtained from Isotec/Sigma-Aldrich. $^{17}O_2$ at 28.8% isotopic enrichment was obtained from Icon Isotopes (Summit, NJ). All chemicals were used without further purification. Site-directed mutagenesis of YvrK active site tyrosyl residues Tyr-200 (N-terminal site) and Tyr-340 (C-terminal site) to phenylalanine was carried out using the QuikChange kit from Stratagene (La Jolla, CA), and the construct sequence verified using the services of the University of Florida Interdisciplinary Center for Biotechnology Research. Mutagenic primers were obtained from Integrated DNA Technologies, Inc (Coralville, IA).

Preparation of Native and d_4-Tyr-labeled Oxalate Decarboxylase—Isotopically neutral YvrK protein was overexpressed, purified, and assayed as described (4). Protein concentrations were measured by the method of Lowry (12). Incorporation of ring-deuterated tyrosine was achieved by growing cells in M9 minimal medium supplemented with 50 mg/liter phenylalanine, 35 mg/liter tryptophan, 5 mg/liter tyrosine, and 1 g/liter *N*-(phosphonomethyl)glycine (glyphosate) to inhibit *de novo* biosynthesis of aromatic amino acids (13). The culture was initiated with a limiting concentration of unlabeled tyrosine rather than the isotopically labeled form in order to minimize the possibility of deuterium incorporation into other amino acids through metabolic scrambling during biomass accumulation. Medium was inoculated with a freshly transformed single colony of bacterial cells and shaken at 250 rpm at 37 °C. When the cell culture started to leave the exponential growth phase, because of limiting tyrosine (OD_{600} ~0.8), 50 mg/liter of L-4-hydroxyphenyl-2,3,5,6-d_4-alanine (d_4-tyrosine) was added. Since the yield of expression and specific activity of OxDC depends on the ability of cells to express heat shock proteins before induction (2), the culture was allowed to reach exponential growth phase again (OD_{600} ~ 1.2) before heat-shocking at 42 °C for 18 min and subsequent addition of isopropyl β-D-galactothiopyranoside and $MnCl_2$ to final concentrations of 1 and 5 mM, respectively. Addition of $MnCl_2$ caused formation of a white precipitate, most likely the manganous glyphosate complex. Cultures were harvested by centrifugation after 3 h of induction at 37 °C, and enzyme manipulated and purified as for the unlabeled protein.

Tryptic Digestion and Mass Spectroscopy—d_4-Tyrosine incorporation was verified by tryptic digestion of labeled YvrK and mass spectral analysis of the fragments. Purified OxDC (18 μg) was loaded onto a 12% SDS-polyacrylamide gel, and prepared according to protocols supplied with the ProteoProfile kit. The mass profile of the peptide mixture thus prepared was analyzed on a PerSeptive Biosystems Voyager DE-PRO matrix-assisted laser desorption ionization time-of-flight mass spectrometer at the Protein Chemistry Core Facility, Biotechnology Program, University of Florida.

Preparation of Samples for EPR Spectroscopy—Unless otherwise noted, EPR sample pH was buffered with 50 mM sodium acetate at pH 5.2. Enzyme preparations were dialyzed, chromatographed over G-25 size exclusion resin, or diafiltered to remove free manganese. Reactions were initiated by addition of oxalate or an analog of oxalate, if present. After transfer of the necessary reaction components to the EPR sample tubes, samples were frozen within 1–2 s by immersion into an isopentane bath prepared by cooling with a secondary liquid nitrogen bath until rapid nitrogen boiling subsided. Aerobically prepared samples were sealed with clay or wax in order to prevent condensation of liquid oxygen in the sample tube during spectral acquisition.

$^{17}O_2$ was received from the supplier in breakseal flasks. A working stock of gas was prepared by attaching via needle-terminated Tygon tubing the breakseal flask along with a small stainless steel bearing to a round-bottomed flask of approximately equal volume sealed with a rubber septum (Supplemental Fig. S1*A*). The receiving flask and Tygon tubing were evacuated with a second needle attached to the vacuum manifold and inserted through the rubber septum. After this second needle was removed, the glass seal was broken by a sharp blow with the bearing. $^{17}O_2$ was condensed into the round bottom flask by cooling with liquid nitrogen. After transfer, the needle and tubing were removed and the sealed flask warmed back to room temperature. To make a gas mix resembling an aerobic environment, four volumes of nitrogen gas and one volume of enriched $^{17}O_2$ were syringed into an evacuated flask of appropriate volume (Supplemental Fig. S1*B*).

For anaerobic samples or those containing $^{17}O_2$, enzyme was mixed aerobically with all reagents except oxalate and $^{17}O_2$, transferred to a 3-mm inner diameter EPR tube, and flash-frozen by liquid nitrogen immersion before attachment to a vacuum/argon double manifold by a short length of standard rubber vacuum tubing (Supplemental Fig. S1*C*). The EPR tube headspace was exchanged for argon by three pump-vent cycles. Enzyme solution was allowed to degas by thawing under argon. This procedure was performed three times before addition of other reagents. $^{17}O_2$ was transferred to the degassed enzyme solution by first flame-sealing the EPR tube containing frozen and evacuated enzyme + buffer, then attaching this tube to vacuum tubing connected to a sealed round-bottom flask containing either $^{17}O_2$ (28.8% enriched) or 20% $^{17}O_2$/80% N_2 (Supplemental Fig. S1*C*). Subsequent breakage of the EPR tube by gentle pressure with pliers permitted exposure of the frozen enzyme solution to the alternative gas mixture (Supplemental Fig. S1*D*). Enzyme was thawed and left to equilibrate with the headspace for 30 min before freezing and transfer back to the manifold. Oxalate was added by disconnecting the EPR tube from the manifold under argon flow, adding the necessary volume of degassed oxalate stock solution by syringe, temporarily sealing the tube and shaking all liquid to the bottom of the EPR tube to mix, then quickly reattaching the tube to the manifold, and freezing to quench the reaction. The headspace was then evacuated and the tube flame-sealed for spectral analysis.

Samples to test the effects of D_2O on the radical spectrum were prepared with buffer and substrate stock solutions containing 99% isotopically enriched D_2O instead of H_2O. The hydrogen ion concentration of buffer and oxalate stock solutions was adjusted with HCl or NaOH, however. The equivalent sample pD should thus be 5.6 because of the equilibrium deuterium isotope effect on protonation and the use of protium at the reference electrode (14). This difference is expected to be relevant only for quantitation, not the qualitative line shape analyses performed here as discussed under "Results" for isotopically neutral samples at pH 7. Enzyme was diafiltered into deuterated storage buffer (20 mM hexamethylenetetraamine, pD 6.4; 0.5 M NaCl) through a Microcon YM30 (Millipore, Billerica, MA). We estimate the exchange efficiency and final deuterium enrichment to be ≥98%.

Temporal Evolution of the YvrK Radical Signal under Turnover Conditions—A 5-ml reaction mixture was prepared containing 2 mg/ml YvrK, 50 mM potassium acetate buffer pH 5.2. The reaction was begun by addition of potassium oxalate to 100 mM final concentration. Aliquots (500 μl) were quenched at different times by cryogenic flash-freezing for EPR samples, or by adding NaOH to 0.1 M final concentration for oxalate consumption measurements.

Radical Quenching in the Frozen State—To measure the lability of the observed radical in the temperature range used for "high-temperature" spectral acquisition, a sample of enzyme undergoing turnover was flash-frozen 2 min after introduction of substrate oxalate. The temperature was raised to 100 K, a reference spectrum taken, and radical intensity monitored for 30 min at each temperature 120, 130, 140, 150, 160, 180, and 200 K. Single scans were acquired at 0.6 milliwatts with a 10 G modulation amplitude and a 10.5 s sweep time.

To rule out temperature broadening or reversible chemical processes as the cause of the decreased signal intensity, after acquiring the last scan at 200 K, cryostat temperature was lowered to 100 K and a spectrum acquired under the same conditions as at the beginning of the experiment. The sample was then thawed briefly and refrozen to test for continued turnover. The presence of an intensified radical signal relative to that seen in the final 200 K scan confirmed the presence of oxalate in the solution, showing that the enzyme was initially frozen under turnover conditions prior to complete consumption of substrate.

Spectral Acquisition and Analysis—CW perpendicularly polarized X-band spectra were acquired on either a Bruker Elexsys model E580 spectrometer operating in TE101 mode, or a Bruker model ECS106 with a dual-mode cavity operating in TE102 mode. Temperature control on both instruments was maintained with an Oxford Instruments model ESR900 helium flow cryostat coupled to an Oxford ITC 503 temperature controller. Parallel polarization spectra were measured in the ECS106 operating in TE012 mode. Simulations were done with the EasySpin toolbox (15) in combination with the MATLAB computing environment (The MathWorks, Natick, MA), and with programs written by one of the authors (A. O.).

Time course data for the development and decay of the YvrK radical were numerically simulated to test potential kinetic models using the program package Gepasi (16–18). The rate constants thus derived were compared with the turnover number in EPR samples, which was cal-

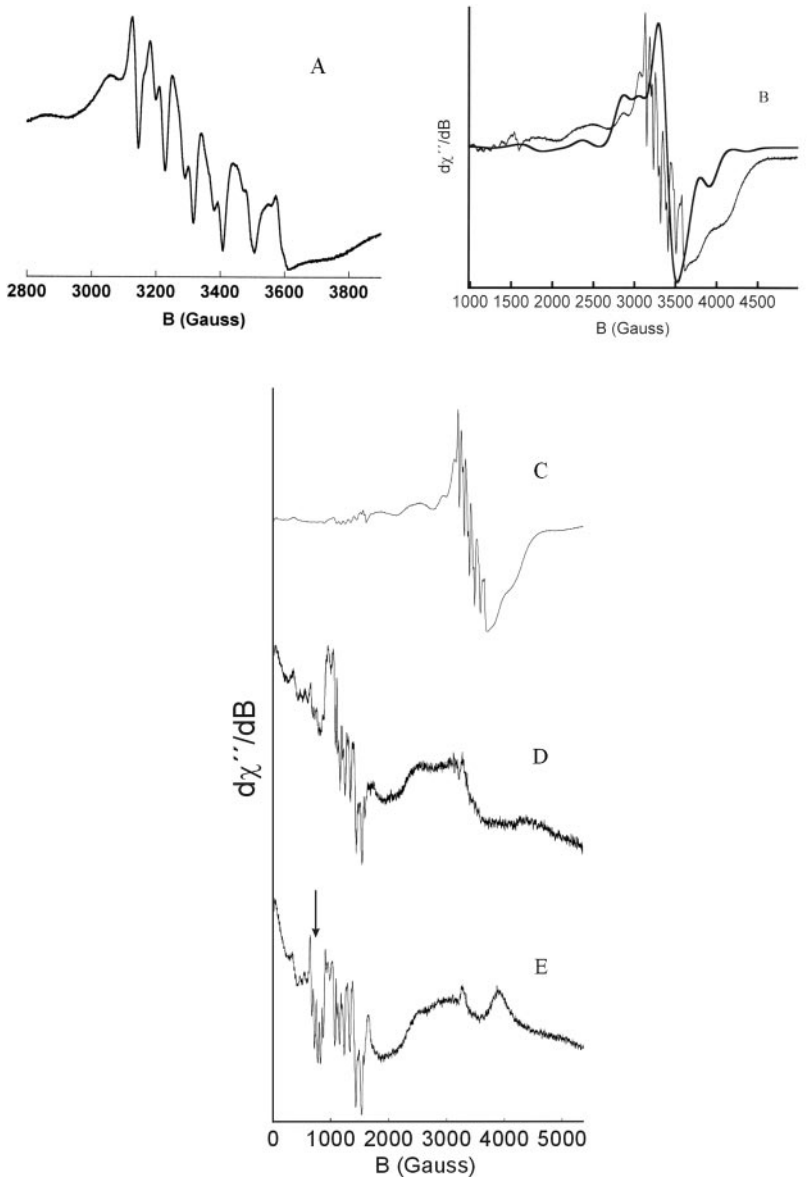

FIG. 1. *A*, narrow scan continuous-wave X-band spectrum of the central-field manganese transition in resting state, as purified YvrK. *B*, overlay of the full experimental spectrum shown partially in (*A*) (*light line*) with a simulation (*dark line*) of the broad features arising from a small zero-field splitting. Parameters used were g_{iso} = 2.0034, ν = 9.437713 GHz, D = 0.023 cm^{-1}, and a 100 G Gaussian line width; hyperfine interactions were not included in the spin Hamiltonian. *C*, freshly frozen, anaerobically prepared YvrK and oxalate, perpendicular mode, 3.5 K, 32 milliwatts, six scans. *D*, sample used to obtain spectrum C after storage in liquid nitrogen, parallel mode, 3.6 K, 1 milliwatts, 6 scans; *E*, YvrK combined with oxalate aerobically and frozen after 30 s, followed by storage at 77 K until acquisition, parallel mode, 3 K, 20 milliwatts, 4 scans. Modulation amplitude was 10 G in all spectra. An additional feature at ~800 G can clearly be seen in spectrum (*E*) (*arrow*), consistent with formation of Mn(III) during extended incubation at liquid nitrogen temperatures. Spectrum (*C*) is essentially the same as in parts (*A*) and (*B*), but is aligned separately with spectra (*D*) and (*E*) for clarity. The small feature near 3300 G in subfigures (*D*) and (*E*) is caused by a persistent background cavity signal.

culated based on the initial slope of a plot of [formate] *versus* time.

Resolution enhancement of the high temperature radical signal was performed with software written in the Reed laboratory (19). For measurement of $P_{½}$, the radical signal intensity was taken as the magnitude of the peak-to-trough difference. Data were transformed and plotted to fit parameters of the standard Equation 1 (20–22),

$$\log \frac{S}{\sqrt{P}} = \log K - 0.5b \log\left(1 + \frac{P}{P_{½}}\right) \qquad \text{(Eq. 1)}$$

where S is the peak-to-peak derivative signal amplitude, P is the microwave power, K is a factor accounting for vertical displacements of the plot and depends on the sample and instrument (22), b is an inhomogeneity parameter varying from 1 (completely inhomogeneous broadening) to 2 (completely homogeneous broadening), and $P_{½}$ is the characteristic half-saturation power of the signal. Fitting was done with the commercial plotting package Kaleidagraph (Synergy Software, Reading, PA).

RESULTS

The Manganese Centers in B. subtilis Oxalate Decarboxylase—The OxDC from *B. subtilis* has been previously demonstrated to be a manganoenzyme as purified from an *Escherichia coli* overexpression system (2, 3) As expected, the X-band spectrum of the resting state enzyme in perpendicular mode shown in Fig. 1, *A–C* displays a sextet pattern centered at g = 2.003 characteristic of the hyperfine-split $M_S = -½ \leftrightarrows +½$ central-field transition of Mn(II). The shoulders on the main central field sextet at magnetic fields of ~3060 G and 3700 G arise from transitions between fine structure sublevels other than the central field transition, and are broadened relative to the central field line due to the greater anisotropy of transitions between outer M_S levels (23). Simulation of these and other broad lines apparent in the spectrum shown in Fig. 1, *A–C* assuming only an axial zero-field splitting component provides an estimate for D of 0.023 cm^{-1} (Fig. 1*B*). In addition, observation of the distinctive sextet feature present near g = 4.3, which we attribute to a half-field transition (24), implies modest zero-field splitting well below the X-band energy of 0.3 cm^{-1}. The hyperfine splitting of the half-field transition was measured as 94 G, essentially the same as that seen for the central field line (93 G). The presence of the half-field line and the magnitude of the hyperfine splittings are consistent with a single environment of octahedral coordination of manganese; we note that a second binding environment for manganese to account for the half-field line is not necessary, as was suggested earlier (2). Likewise, the apparent splitting of the hyperfine lines of the $g \sim 2$ signal evident in Fig. 1*A* is well precedented, and understood to arise in a single molecular

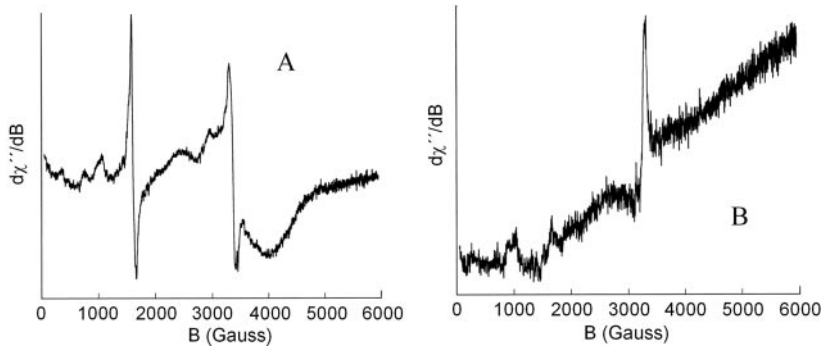

FIG. 2. **The EPR spectrum of YvrK after overnight turnover.** *A*, perpendicular, 10 milliwatts; *B*, parallel, 32 milliwatts. Small features between 1000 and 2000 G in the parallel mode spectrum are identifiable as arising from molecular oxygen. Both spectra were taken at 6 K with 10 G M.A., and are the averages of 4 scans. The feature at 3300 G in *B* is a background signal due to the spectrometer cavity.

environment from forbidden $\{\Delta M_S = \pm 1, \Delta M_I = \pm 1\}$ transitions that gain intensity through the small axial zero-field splitting coupling to the hyperfine transition intensity in second and third order perturbation theory (25, 26). Notably, the intensity of the higher-field hyperfine line (sharp peak just below 3600 G in the spectrum of Fig. 1*A*) is slightly greater than the others immediately downfield. This may be compared with the identical feature seen for Mn(II) bound to the hammerhead ribozyme as contrasted with free $Mn(H_2O)_6^{2+}$, the latter complex showing a more equitable distribution of intensities across this high field hyperfine triplet (26, 27). This observation supports protein-bound rather than freely solvated manganous ions as the source of the EPR signals reported herein.

Manganic ion often exhibits parallel mode EPR signals at apparent free electron *g*-values near 8–9 (~800 G at X-band), as can be seen in the spectra of salicylidenato Mn(III) and acetylacetonato Mn(III) (28, 29), and in the spectrum of oxidized manganese-dependent superoxide dismutase (30). When OxDC is mixed anaerobically with oxalate, such that no turnover may occur, a variety of lines in the parallel mode spectrum with the characteristic sextet splitting of manganese are evident below fields of ~1500 G (Fig. 1*D*), which may be attributed to greater transition intensity of the half-field line when $B_1 \parallel B_0$. In some cases, the presence of oxygen together with oxalate leads to an additional sextet at ~800 G (Fig. 1*E*), suggestive of manganic ion. It was noticed that during the time between preparation and EPR analysis of the two samples used to obtain these spectra (Fig. 1, *D* and *E*), quenching of the organic radical species (observed in freshly prepared samples) took place after overnight storage at 77 K, with the concomitant appearance of a sextet at ~800 G. From these observations, we conclude that slow radical quenching at 77 K is associated with formation of Mn(III) under these conditions. The absence of a spectral signature for manganic ion in freshly prepared, aerobic samples can be explained by the hypothesis that Mn(III) intermediates at physiological temperatures are either short-lived or not formed during steady-state catalytic turnover. Another possibility is that Mn(III)-containing enzyme has zero-field splittings that are too large to allow observation at X-band frequencies (see below).

Overnight incubation of enzyme and substrate under aerobic conditions prior to freezing and immediate spectral acquisition led to the spectra shown in Fig. 2. The perpendicular mode spectrum (Fig. 2*A*) shows an intense $g = 4.30$ feature lacking obvious sextet splitting. This feature is also seen in samples that are incubated for shorter times, but which are annealed at 120–160 K prior to spectral acquisition at lower temperatures (4–10 K). In contrast, the parallel mode spectrum (Fig. 2*B*) is devoid of features in this spectral region. Besides the $g = 4.30$ feature, the perpendicularly polarized spectrum of the manganese signal in enzyme incubated overnight with oxalate shows a dramatic change in the central field region near $g = 2$. A much broader signal with its peak and trough centered at 2500 and 4000 G, respectively, can be observed, and the hyperfine-split central field transition seen in resting enzyme samples has been replaced with a narrower, almost featureless line at $g = 2.06$ (Fig. 2*A*). The peak-to-peak width of 120 G differs from that of the $g = 4.30$ feature (80 G), suggesting that the latter may not be a half-field transition related to the former consistent with the relative intensities of the two lines; half-field lines should be less intense than the main line. Rhombic $g = 4.3$ signals have been widely observed at liquid helium temperatures, and are usually attributed to junk iron, or Fe(III) in unknown, generalized ligand fields (31). The enhancement of this signal in our samples could therefore reflect an oxidation process either adventitious over the extended incubation times, or specific because of oxidizing species arising from enzymatic catalysis. However, the concomitant degradation of the manganese central field sextet and appearance of this $g = 4.3$ line suggest the two processes may be linked, and that a change in the manganese ligation environment occurs over the extended incubation times and with the non-physiological oxalate concentrations used here.

Radical Formation upon Oxalate Exposure—A sharp $g = 2.0$ signal with a peak-to-trough width of ~23 G is formed upon exposure of enzyme to oxalate, as shown in Fig. 3. The signal width is too narrow to arise from a transition metal-associated signal, implying that an organic radical is formed during oxalate turnover. Generation of this species required the simultaneous presence of enzyme, oxalate, and oxygen, and was not observed in any of the isolated reaction components. The requirement for the simultaneous presence of O_2, enzyme, and oxalate for both activity (2) and radical formation strongly suggests that the observed species is related to enzymatic catalysis, although not necessarily on the main catalytic pathway. Quantitation against a DPPH standard sample at power levels well below the calculated $P_{1/2}$ (see below) allow an intensity estimate equivalent to ~4% of potential manganese sites in the sample. If manganese occupancy is ~50% as has been previously measured (2), this radical represents ~7% of the active centers present in the sample. Samples containing formate and bicarbonate in lieu of oxalate did not show a radical species, consistent with the presence of an effectively irreversible step subsequent to the production of the radical species in the forward reaction. Finally, the ability to form the $g = 2.0$ radical was not affected in the Y200F, Y340F, or Y200F/Y340F site-directed variants, arguing against adventitious radical formation in the active site by wayward reaction intermediates.

Radical Presence under Non-turnover Conditions and Intensity Variation with Time—Notably, the narrow $g = 2.0$ paramagnetic species is formed at pH 7 in potassium-BES buffer, a condition under which the enzyme does not turn over significantly. Although not definitive evidence of catalytic irrelevance, this result alone might suggest that the radical formed is auxiliary to the primary catalytic pathway active at the pH optimum of the enzyme. Alternatively, a stable radical might

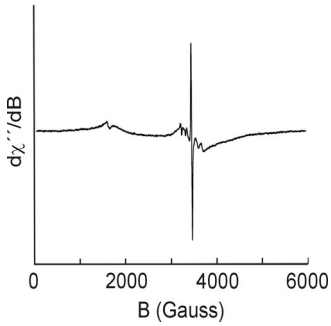

FIG. 3. **EPR spectrum of YvrK frozen 30 s after oxalate addition.** Perpendicular mode, 5 K, 0.1 milliwatt, 4 scans. Sample was 150 μM YvrK subunits, generated by addition of 100 mM potassium oxalate pH 5.2. Quantitation *versus* a 24 μM diphenylpicrylhydrazyl standard allows an intensity estimate corresponding to 2–5% of the manganese sites.

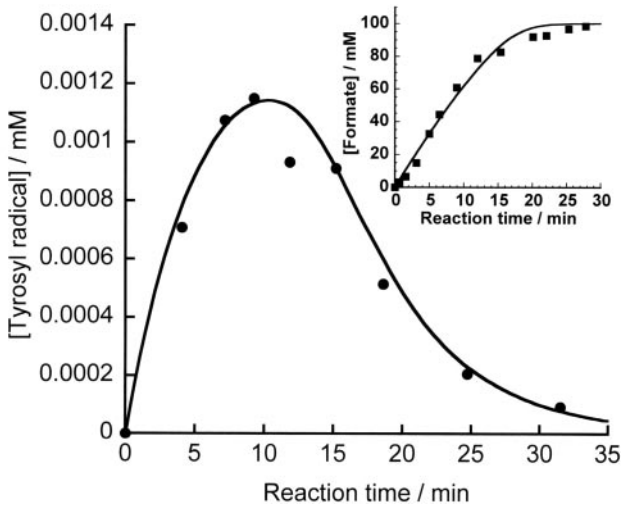

FIG. 4. **The steady-state YvrK radical intensity as a function of reaction time.** Intensity was calculated from double integration of the simulated radical signal and comparison with a DPPH concentration standard. Reaction conditions were 0.5 M piperazine/piperazine·H^+ pH 5.2, $[oxalate]_0$ = 100 mM, [OxDC] = 15.9 μM. All spectra were taken at 4 K with 0.2 milliwatts microwave power, 10 G M.A., and were the sum of 4 scans. *Inset*, formate as a function of reaction time. Data were simulated (*solid lines*) according to the kinetic mechanism presented in Scheme 2.

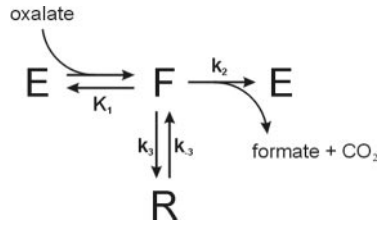

SCHEME 2. Kinetic model for the steady-state radical observed during OxDC catalysis. *E* is free enzyme, *F* represents all kinetically equivalent enzyme species on the catalytic pathway, and *R* is the form of the enzyme containing the observed steady-state radical. Kinetic constants from numerical simulations using this general mechanism are k_2 = 632 ± 1.7 min^{-1}; k_3 = 0.020 ± 0.001 min^{-1}; and, k_{-3} = 0.16 ± 0.01 min^{-1}. The enzymatic k_{cat} of 420 min^{-1} implies that radical formation is not kinetically competent and thus not on the main catalytic pathway.

be formed by a single turnover of enzyme that is then blocked by the absence of a suitable proton donor, the accumulation of the radical species at lower pH would reflect its relative thermodynamic stability, whereas its persistence at higher pH would reflect a blockage during catalysis (and its stability relative to whatever quenched forms are available to it at the higher pH). In order to test this, enzyme was exposed to a single subunit-equivalent of substrate under turnover conditions. An intense signal was found well after all substrate would have been consumed. Because the paramagnetic species cannot be formed from exhausted substrate, and since signal is absent when products alone are present (see above), the species must be stable on a time scale of minutes. This suggests the process of radical formation is not associated with the proton-sensitive rate-limiting step because if it were the radical would have been quenched completely after a single enzymatic turnover to products. Production of the radical then likely occurs prior to the rate-limiting step, and thus without further evidence could be associated with an activation step that is necessary prior to steady-state turnover.

A more thorough examination of radical intensity and substrate consumption *versus* time (Fig. 4) shows development of both to be at least biphasic. Radical intensity increases monotonically during steady-state turnover, and peaks approximately as turnover becomes substrate-limited. As formate production approaches its asymptotic limit, the radical decays back toward zero intensity. In addition, the line shape of the signal was observed to become gradually narrower as the signal decayed, possibly reflecting a distribution of hyperfine couplings arising from multiple radical conformations.

To extract an approximate rate of radical formation, we numerically simulated several potential kinetic mechanisms. The solid lines overlaid on the radical intensity data and formate concentrations of Fig. 4 represent the simulated intensities and concentrations, respectively, of the simplest model that simultaneously fit both data sets, shown in Scheme 2. The only explicit constraints on the model were the initial oxalate concentration of 100 mM and the enzyme concentration in the EPR samples. K_1 is not a simple dissociation constant but instead reflects all forward and reverse rate constants up to the hypothetical branch point in which the steady-state radical is formed. Numerical simulation gave a value of 14 mM for K_1; however, the dependence of the overall model on this value was found to be low as reflected by large standard deviations in the constituent effective rate constants k_1 and k_{-1}. Thus, the particular value for K_1 has little chemical meaning or kinetic consequence. On the other hand, first-order rate constants for radical formation and decay within the model presented in Scheme 2 were found to be k_3 = 0.02 ± 0.001 min^{-1} and k_{-3} = 0.16 ± 0.013 min^{-1}, respectively. The former is of special interest in connection with overall enzymatic turnover.

If the presence of the radical is required during the catalytic cycle, either directly or indirectly as a marker for an obligate intermediate, then it is expected that the radical intensity should be proportional to the rate of change of oxalate with time, *i.e.* the slope of the formate production curve should increase as more radical is formed. This is not the case, as seen in the Fig. 4, *inset*; the magnitude of the slope in the Fig. 4, *inset* is maximal at zero time, whereas the radical reaches maximum intensity only after 10 min. Although the formate concentrations at early time points might suggest a positive curvature and thus an activation process, the inflection of the [formate] *versus* time curve does not occur at the maximum of radical intensity, as would be expected. We therefore do not believe the radical species represents a by-product of an obligatory activation process. In addition, k_{cat} under the experimental conditions is calculated to be ~420 min^{-1} based on the slope of the Fig. 4, *inset* at t = 0. The rate of primary radical formation (0.02 min^{-1}) is thus approximately four orders of magnitude lower, ruling out its participation as a kinetically competent intermediate in the reaction mechanism. The existence of a paramagnetic intermediate is of course not ruled out by the present study; however, if present it is not the steady-state

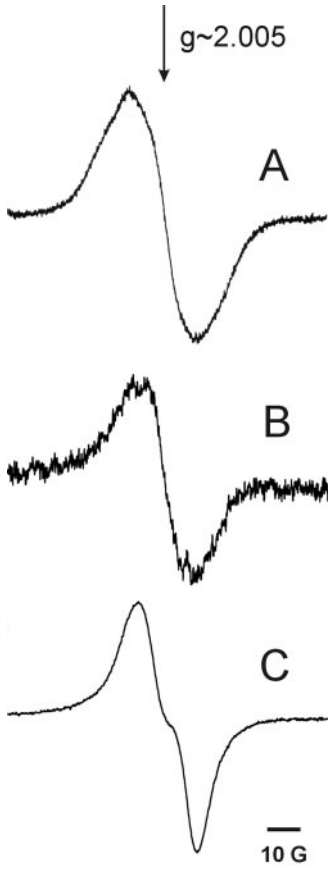

FIG. 5. **Effects of temperature and isotopic editing on the observed radical spectrum in OxDC.** *A*, 5 K without isotopic editing, 1 G M.A., 0.1 milliwatts, 4 scans. *B*, 160 K without isotopic editing, 2 G M.A., 2 milliwatts, 10 scans. *C*, 120 K with enzyme containing tyrosine residues uniformly on the ring with deuterium, 4 G M.A., 0.8 milliwatts, 16 scans. Higher temperatures allow sufficient motion for partial averaging of hyperfine anisotropy, narrowing the hyperfine lines, and allowing subtle features to be observed that would be hidden at lower temperatures.

radical, nor does it accumulate to observable levels during steady-state turnover under these experimental conditions. Observation of more stable radicals in lieu of less stable, kinetically competent species is not unprecedented in enzymatic systems with free radical intermediates, as will be discussed further below.

Effect of Temperature and Isotopic Editing on Radical Spectrum and Resolution Enhancement—Fig. 5 shows the spectra observed at low temperature without isotopic editing (Fig. 5*A*), at 160 K without isotopic editing (Fig. 5*B*), at 120 K with uniformly d_4-Tyr-labeled YvrK (Fig. 5*C*). At higher temperatures additional structure can clearly be seen, consistent with increased molecular motion averaging out hyperfine anisotropy and the associated broadening that manifests at lower temperatures (32). Replacement of protons on enzymic tyrosine residues with deuterons results in clear narrowing of the high temperature signal, such that an inflection point can be observed in Fig. 5*C*. Mass spectral analysis confirmed the presence of a single species with a mass consistent with uniform [d_4-Tyr] labeling, demonstrating that labeling of YvrK was essentially complete and that no secondary labeling was achieved by metabolic scrambling of the supplied tyrosine. A larger splitting still remains after deuterium substitution, and substitution of exchangeable protons with deuterons does not narrow this radical spectrum detectably, suggesting the remaining doublet coupling evident in the [d_4-Tyr] YvrK radical spectrum arises from coupling to one or both β-methylene protons. This interpretation is consistent with the spectral changes observed by Tommos *et al.* (33) for the $Y_Z^{\cdot}$ radical of manganese-depleted photosystem II upon selective deuteration of ring carbons 3 and 5.

In much the same way that nuclear magnetic resonance signals can be sharpened by appropriate apodization and zero-filling in the time domain prior to Fourier transform into the frequency presentation, continuous wave EPR spectra may be reverse-Fourier transformed to the time domain and processed analogously (19). Although the enhancement process sacrifices some of the relative intensity information, the processing is invaluable in teasing out splittings hidden by inhomogeneous broadening. The result for the high temperature radical signals are shown in Fig. 6. The spectrum of unlabeled YvrK after resolution enhancement (Fig. 6*A*) confirms the presence of underlying hyperfine structure in the observed radical signal. Most of this structure collapses upon tyrosine deuteration (Fig. 6*B*), consistent with the 6-fold lower gyromagnetic ratio of deuterium relative to protium, leaving a single apparent coupling. The presence of D_2O did not change the linewidths or shape of the EPR spectra from unlabeled or deuterated protein.

At temperatures near 200 K the radical was observed to quench rapidly, consistent with increased protein flexibility allowing electron transfer to or from this radical. As noted above, EPR features consistent with Mn(III) were found in quenched samples, suggesting the active site metal center(s) as a potential source of electrons. Notably, in experiments in which the reaction is frozen within a few minutes after oxalate addition and then annealed, the radical re-forms upon thawing, brief incubation, and re-freezing, and likewise anneals at high temperature (data not shown). Repeated cycles in this fashion eventually fail to produce a radical signal because all oxalate has been consumed, but upon addition of a small amount of oxalate the signal reappears. This behavior clearly illustrates a connection between radical formation and enzymatic turnover. Frozen annealing does not permit exchange of products and substrates between the enzyme active site(s) and the bulk medium, but allows the radical to quench through enhanced molecular motion and interaction with a redox-active species. Upon thawing, fresh oxalate can bind to the enzyme, and initiate further turnover with concomitant production of the radical species.

The instability of the observed radical species even in frozen samples was intriguing, and the temperature dependence investigated further. The tyrosyl radical was generated by limited enzymatic turnover, and a sample frozen for spectral analysis. Cryostat temperatures were slowly raised in 10–20 K steps, and radical signal intensity monitored in time. Contrary to finding a temperature at which the radical decayed completely to zero, or temperature dependence of a single observed quenching rate, the radical signal intensity was found to quench quickly and irreversibly, but only partially as temperature was raised, reaching an asymptotic intensity at each temperature. Upon lowering the cryostat temperature to 100 K, where radical signal intensity was not observed to decrease with time relative to 10 K spectra, signal intensity did not recover thereby ruling out temperature broadening as an explanation. The existence of asymptotic values of radical concentration that decrease as temperature is raised suggests that only subpopulations of the radical quench at each temperature. The implications of this interpretation will be discussed below.

Power Saturation of Signal—The response of radical signal intensity to applied microwave power at 10 K shown in Supplemental Fig. S2. Fitting to Equation 1 gives a characteristic half-saturation power of 1.1 ± 0.1 milliwatts and an inhomogeneity parameter value of 1.34 ± 0.02. These values are con-

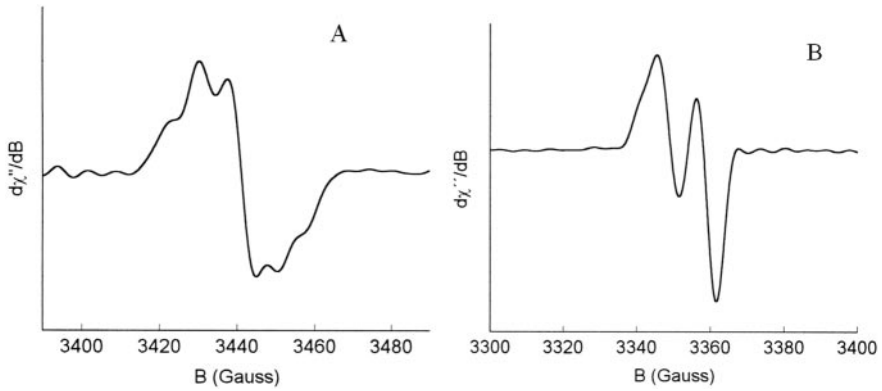

FIG. 6. **Resolution enhancement of spectra presented in Fig. 5*A* (*A*) and Fig. 5*C* (*B*).** The resolution enhancement procedure can be seen to be particularly valuable in rigorously deconvoluting the spectrum of Fig. 5*C* into a simple doublet; without the procedure, the positive derivative half of the spectrum that is slightly broader than the negative half might be interpreted as containing additional splittings.

sistent with an organic radical, as is discussed further below. The quality of the fit in Supplemental Fig. S2 suggests that barring radicals with identical relaxation properties, only one radical species is present at the reaction time examined here (≤2 min). This fact greatly facilitates interpretation of line shapes and mechanistic relevance presented below.

DISCUSSION

Nature of the Manganese Center in Oxalate Decarboxylase—The hyperfine splitting and prominent isotropic $g \sim 2$ signal in the CW-EPR spectrum of resting-state YvrK is consistent with octahedral coordination (25), as is expected from the crystallographic structure. The Mn(II) hyperfine lines seen on the $g \sim 2$ signal arising from the $M_S = -½ \leftrightarrows M_S = +½$ fine structure transition occur in pairs. Although this could arise due to slightly different *g*-values associated with the two manganese sites in each enzyme subunit, our observed spectrum in the resting state is very similar to that seen from manganese bound to the high affinity hammerhead ribozyme site (26). These hyperfine line doublings are generally interpreted as arising from forbidden ($\Delta M_S = \pm 1$, $\Delta M_I = \pm 1$) transitions that gain intensity by virtue of a slight breakdown of the selection rule via coupling between the hyperfine interaction and the zero-field splitting parameters in higher orders of perturbation theory (25). The observation of the half-field line and the presence of prominent shoulders in the manganese spectrum because of transitions among the higher M_S manifolds suggest a modest zero-field splitting for the manganous form of OxDC as purified. Such a splitting is consistent with the nearly octahedral coordination observed in the structure. Similar spectral features were observed in resting state barley oxalate oxidase, the EPR spectrum of which is also consistent with octahedral coordination in the absence of iodide anions, the latter giving rise to a spectrum suggesting pentacoordination (34).

Although isotropic hyperfine splitting arises from electron spin density at the nucleus of the ion in question (Mn(II), in this case), it is telling of the coordination environment by virtue of the differential ligand repulsions in different coordinations and their effect on the spin density distribution of the central ion. So, octahedral environments tend to yield Mn(II) hyperfine couplings of ~95 G; the reduced interelectronic repulsion of a tetrahedral environment, which allows spin along with total electron density to expand away from the central nucleus relative to the octahedral case, produces metal-centered hyperfine splittings of around 70 G at X-band frequencies (25). Metal-ligand covalency can alter these numbers significantly; however, the O/N ligand environment around the high-spin YvrK manganese ions are not associated with large covalency. The 93 G splitting observed for resting YvrK indicates octahedral coordination. In recombinant, heterologously expressed oxalate oxidase as examined by Whittaker and Whittaker (34), the hyperfine lines are partially resolved; they appear more distinctly upon anaerobic addition of oxalic acid together with increased modulation depth. In our hands, *B. subtilis* OxDC exhibits the opposite effect upon oxalate addition, suggesting that either the nature or lifetimes of metal-associated intermediates may be different between the two enzymes.

The parallel polarization data do not lend support to a resting Mn(III) or Mn(IV) state in the recombinant protein as purified, or to the existence of a long-lived, high-valent state during steady-state turnover. However, if a high-valent manganese species were formed that underwent significant Jahn-Teller distortion, it is conceivable that the associated change in magnitude and possibly rhombicity of zero-field splitting would be large enough such that the anticipated signal with parallel microwave polarization would be broadened beyond detection. Thus, while parallel polarization data do not directly support high-valent manganese participation, it cannot be ruled out on the basis of these measurements. We note, however, that the resting enzyme is nearly colorless in our hands, suggesting little Mn(III) or Mn(IV) content, and no visible color is developed in reaction mixtures upon oxalate addition. There is therefore an absence of a *stable* Mn(III/IV) intermediate in the OxDC catalytic cycle similar to that which persists in Mn-dependent superoxide dismutase after oxidation of the Mn(II) form and production of hydrogen peroxide (30). A discrepancy between the amounts of manganese detected by inductively coupled plasma atomic emission spectroscopy and integration of the manganous EPR signature in an earlier study led to the suggestion that ~20% of the resting state enzyme might be present in the Mn(III) form (2). However, we note that the total width of the divalent manganese signal is very large and possibly spread over many individual broad, low intensity transitions, making quantitation by direct integration exceedingly difficult and unreliable.

The greater intensity of EPR transitions in parallel as compared with perpendicular mode is potentially possible for any system with some degree of ZFS that mixes the Zeeman states. Manganous ion exhibits a particularly rich EPR spectrum in certain ligation environments, and together with evidence of small *D* in the perpendicular mode spectrum the signals we have observed in parallel mode are attributable to Mn(II) rather than the presence of Mn(III). The observation of broad fine structure transitions around $g \sim 2$ is consistent with a small degree of ZFS because in its absence all such transitions would be superimposed (although the greater anisotropy of the non-central transitions broadens these lines), whereas in an environment with large ZFS they would not be observable at all. Furthermore, perpendicular mode EPR showed no trace of Mn(IV) (35–39), which as a Kramer's system is expected to be visible under perpendicular polarization in the absence of large rhombic zero-field splitting. Overall, the EPR data presented and the lack of significant visible absorption support a Mn(II)

center in an octahedral environment with moderate distortion throughout most of the catalytic cycle when considered chronologically, *i.e.* although there may be many intermediates with rhombic or large axial zero-field splittings, including Mn(III) or Mn(IV), they do not accumulate to an observable level and therefore only exist for short times if at all. This behavior of the metal center contrasts with the stability of the Mn(III) center in superoxide dismutase, and might be tied to the different functions of the two enzymes. Thus, OxDC may use the strong oxidant Mn(III) in a purely activating role once oxalate and dioxygen are poised for reaction, whereas the ping-pong kinetics required by the overall superoxide dismutase reaction demand the Mn(III) center in that system to persist long enough for one round of substrate/product exchange. Participation of unpaired electron intermediates in all proposed mechanisms for oxalate decarboxylation to date and the lack of precedent for mononuclear Mn(IV) centers in biology leads us to conclude that if any high-valent species of manganese participate in OxDC catalysis, they will be short lived Mn(III) species.

Features and Behavior of a Tyrosyl Radical in Oxalate Decarboxylase—The equilibrium constant for oxalate decarboxylation based on measured aqueous heats of formation and entropies of oxalate, formate, and CO_2 at 298 K and 100 kPa (40) can be calculated to be between 6.6×10^6 and 1.18×10^{11}. The lower value corresponds to monoprotonated oxalate reacting to give CO_2 and formate, and reflects the greater entropy (more unique atomic configurations due to lower symmetry) available to the monoprotonated form of oxalate than the more symmetric dianion or oxalic acid. The V_{max}/K_m pH profile and heavy atom oxalate isotope effects observed with this enzyme (4) favor a mechanism with monoprotonated oxalate as the enzymatic substrate, and hence the calculated K_{eq} of lesser magnitude; even so, one expects this uni-bi carbon-carbon bond cleavage to be practically irreversible. Depending on the nature of participation of the observed radical in the mechanism, one might expect products to be able to generate the radical species from resting state enzyme. For example, if the rate-limiting step of the reaction were quenching of a putative formate σ radical centered on carbon, a hydrogen abstraction or proton-coupled electron transfer from formate would not be out of the question. Nevertheless, no radical signal was observed when formate and bicarbonate were added to YvrK, ruling out a stable radical intermediate that persists at observable concentrations after the establishment of reaction equilibrium and arguing against a reversible net hydrogen atom transfer to formate as the rate-limiting step.

The featureless signal apparent at low temperatures in YvrK treated with substrate and dioxygen develops clear structure at higher temperatures. Isotopically enriched oxalate showed no detectable coupling between the radical signal and ^{13}C, eliminating a metastable oxalyl or even formyl intermediate as a possibility for the paramagnetic site. Enrichment of cofactor dioxygen with ^{17}O also produced no change in spectral line shape. Peroxyl radicals typically exhibit axial spectra with a distinctive negative component larger than the positive components in the derivative presentation (41, 42); together with the isotopic data, a radical centered on O_2 also appears unlikely. Thus, both the radical formation rate and isotopic labeling of substrates and cofactors argue against direct radical participation as an intermediate species.

Having eliminated known reaction participants, the most likely alternative identity for the radical host is a protein residue. The OxDC radical observed manifests additional structure at higher temperatures that might give easy clues to its identity. Unfortunately, the radical quenches at temperatures that might allow more clear manifestation of motionally averaged hyperfine structure, thereby limiting the available signal-to-noise ratio. Nevertheless, several lines of evidence establish this species as a tyrosyl radical. First, the lineshapes at low or higher temperatures are inconsistent with other radicals that have been observed in proteins, such as glycyl (43), cysteinyl (44), or tryptophanyl (45, 46). Some similarity exists between the spectral envelope of the present species and that of a sulfinyl radical observed during oxygen-dependent inactivation of pyruvate-formate lyase (47), and that seen in the Y177F/I263C double mutant of murine type 1 ribonucleotide reductase R2 protein (48); however, three pieces of evidence argue against this possibility in the case of OxDC. First, sulfinyl radicals reported show a relatively large g_x value of ~2.02; our spectra cannot be simulated with a value this large. Furthermore, there is only one cysteine residue in the YvrK gene product (Cys-383), which is distant from either manganese ion and mobile enough to have not been seen in the electron density map during structural determination (3). Finally, the C383S protein variant formed the observed radical at a level and rate similar to unaltered enzyme (data not shown). The radical is observed only upon oxalate exposure, is quenched within 30 min of oxalate depletion, and can be restored by further oxalate addition, behavior that does not lend itself to an adventitious cysteine sulfinyl radical in this case.

A second piece of evidence for a tyrosyl radical comes from resolution enhancement of the high temperature spectrum, which shows multiple splittings underneath the overall envelope of the radical signal. In general, a tyrosyl radical would be expected to show potential magnetic couplings to the hydrogens on the β-carbon of the side chain and to the four ring hydrogen atoms. The enhanced spectrum is consistent with these expectations.

The most convincing and direct evidence comes from spectral narrowing upon deuteration of the tyrosyl ring. Substitution of tyrosyl ring protons for deuterons collapses the observed splittings cleanly, so much so that an inflection becomes visible at high observation temperatures even without resolution enhancement. A similar spectrum was observed for the Y_Z tyrosyl radical of the manganese-depleted *Synechocystis* 6803 photosystem II upon deuteration of the ring positions *ortho* to the hydroxyl group (positions 3 and 5) (33). An especially interesting consequence of this substitution was the difference in relative widths of the positive and negative spectral features; the negative half of the derivative line was noticeably narrower than the positive half, a feature we also observe in Fig. 5*C*. Furthermore, the similarity of the protiated Y_Z spectrum to our resolution-enhanced signal at natural abundance in Fig. 6*A* further supports the assignment of the YvrK steady-state radical species to a tyrosyl residue. The main hyperfine splitting seen in the OxDC d_4-tyrosyl radical of 10 G, as measured by the distance between the first peak and inflection point of Fig. 5*C* or the distance between peaks in resolution-enhanced Fig. 6*B*, is attributable to the remaining β-methylene proton coupling, as deuteration of the phenolic ring removes most of the presumably strong coupling to protons 3 and 5, and the 2,6-coupling in the tyrosyl radical is a small perturbation even with protons at these positions (33). This β-methylene coupling is similar to that observed for *Synechocystis* photosystem II Y_Z (33) ($A^{\beta}_{y,z}$ = 10.4 G, A^{β}_{x} = 12.6 G, Ref. 49), but substantially less than observed in the class I ribonucleotide reductase protein R2 (50) ($A^{\beta}_{y,z}$ = 19.1 G, A^{β}_{x} = 21.8 G, Ref. 49), or the wide doublets of prostaglandin H synthase (51) ($A^{\beta}_{\perp}$ = 20.8 G, $A^{\beta}_{\parallel}$ = 24.6 G (49)). Although the X-band data presented here are of insufficient resolution to permit quantitative analysis of the spin Hamiltonian parameters such as *g*-tensor and hyperfine tensor components, and thus precise numerical simulations,

this 2-fold distinction in the magnitude of the β-methylene hyperfine parameters is sufficient to conclude that the ring torsion of the OxDC tyrosyl radical should more closely resemble that of photosystem Y_Z than of the other radicals. The smaller coupling in the PSII radical arises from a smaller dihedral angle between the ring normal and the bisector of the H_β-C_β-H_β angle. This ring tilt is ~8° in PSII, and ~30° in both RDPR and PGHS-1 (52). We therefore conclude the tyrosyl radical in OxDC has an average conformation with a similarly modest dihedral angle.

The radical quenching we have observed in frozen samples stands in contrast to the behavior of previously reported tyrosyl radicals, and suggests that electron transfer might be responsible for quenching the observed signal at 77 K and below. Examination of a frozen EPR sample at a series of increasing temperatures showed that radical intensity reached a limiting value after each increase. We interpret this to mean that only a fraction of the total radical population quenches at a given temperature, which is consistent with a model in which the tyrosyl radical, together with any functional groups in its surrounding environment that participate in the electron transfer (either directly or as a solvent in the Marcus theoretical sense) samples a set of conformational states within the protein. Thus, at low temperatures, the tyrosyl radical and its motionally coupled environment can adopt an arrangement that is conducive to electron transfer in only a small fraction of protein molecules. Each time temperature is increased, a greater fraction of the proteins can access the conformation required for electron transfer and radical quenching. Therefore at a given temperature the intensity of the radical signal decreases until it reaches an asymptotic value, which corresponds to all of the protein molecules in which the tyrosyl radical does not adopt a conformation suitable for electron transfer.

Three scenarios might give rise to the observed behavior of radical signal intensity: a severely limited set of productive conformations with modest increases in tyrosyl radical conformational sampling as a function of temperature; a tyrosyl residue with extensive conformational freedom freeze-trapped in many orientations during sample preparation; or, an extended electron transfer pathway comprising multiple residues, which must simultaneously be in the correct relative conformations. The EPR spectra of samples frozen before achieving peak intensity suggest a reasonably well defined ring torsion as discussed above, which tends to disfavor the second possibility. However, despite framing the above discussion to include other motionally coupled residues, the choice between the remaining two possibilities awaits identification of the specific oxidized tyrosine.

The fitted half-saturation power of 1.1 milliwatts is lower than would be expected for a transition metal or for a radical tightly coupled magnetically to one. The stable radical formed in ribonucleotide reductase exposed to the cancer therapeutic gemcitabine (2′,2′-difluoro-2′-deoxycytidine) exhibits a $P_{½}$ of 1.0 ± 0.5 milliwatts (22), whereas the tyrosyl radical in the R2 protein that is in close proximity to the dioxo-diferric activating metal cluster has a characteristic half-saturation power of 47 ± 12 milliwatts (53). The latter is greater than the former because of the dipolar-enhanced relaxation provided by its proximity to the diiron center. By analogy, our low measured $P_{½}$ of 1.1 milliwatts suggests that the radical formed in YvrK is relatively isolated magnetically from any manganese center, which may have initiated the immediate reactive precursor. Free tyrosyl radical generated by γ-irradiation of a frozen solution exhibited a $P_{½}$ of 0.64 ± 0.19 milliwatts, and approximately equal amounts of homogeneous and inhomogeneous broadening as illustrated by its inhomogeneity parameter of 1.48 ± 0.17 (54). The $P_{½}$ and inhomogeneity parameter for the radical signal observed with YvrK are comparable to these latter values, but the slightly higher $P_{½}$ might reflect weak coupling to a paramagnet such as manganous ion. Another possibility is a greater variety of molecular environments (different geometries, for example) providing additional relaxation pathways beyond those available to a rigid radical species in a uniform environment.

Potential Functional Implications of the Observed Radical—A tyrosyl radical is conspicuously missing in the proposed mechanisms to date, which are summarized in Supplementary Scheme S1. The necessity for such a species in the catalysis of oxalate decarboxylation is not clear at present, and none of the data presented herein speaks to a requirement for a protein radical in the OxDC catalytic mechanism. However, such a requirement is not ruled out, and there are now several well characterized examples in the literature of enzymes which employ an obligate proteinaceous radical that is only observable as a more stable species. The type I ribonucleotide reductase from *E. coli* forms a catalytic cysteinyl 439 radical in its R1 subunit (55). This radical is formed from hydrogen atom abstraction by tyrosine 122 in the R2 subunit, itself formed by action of the essential diferric cluster. Pyruvate-formate lyase from *E. coli* initiates each turnover from a stable glycyl radical at residue 734, and like the type I ribonucleotide reductase employs the more stable radical as a "holster" for a more reactive one, in this case cysteinyl 419. The *E. coli* type III RDPR employs an analogous scheme, with glycyl-681 (56) serving the role of Gly-734 in the pyruvate formate-lyase (PFL). The sulfur-based radicals do not accumulate during turnover, but instead are seen as the more stable delocalized glycyl or tyrosyl radicals that are corollary to the primary reduction reaction. Only by indirect means have the sulfur-based radicals been observed (57, 58).

Identification of the paramagnetic species as a tyrosyl radical advances mechanistic reasoning substantially. The radical forms only under turnover conditions, which might imply that a residue near the active site is involved. However, as discussed above, an obligatory radical-mediated activation or participation of the observed radical as a reaction intermediate contradicts the data. Furthermore, the unimpeded formation of radical in Y200F, Y340F, and Y200F/Y340F active site variants together with the modestly perturbed half-saturation power imply some distance between the radical and the active-site manganese ions. A seemingly well defined tyrosyl ring torsion angle does not support radical formation on the protein surface, which could arise from nonspecific oxidation by reactive side products. Indeed, the data taken together raise the possibility of long-range electron transfer through the polypeptide framework. Parallel polarization EPR signals near $g = 8{\sim}9$ consistent with Mn(III) together with apparent radical quenching in cryogenically aged samples under turnover conditions suggest potential redox coupling between the radical and one or both manganese sites in the protein. Under turnover conditions when the radical has not had an opportunity to quench, however, the absence of any Mn(III) or Mn(IV) signals concomitant with radical concentrations approaching 10% of manganese binding sites means that tyrosine oxidation is not accompanied by formation of either high valent manganese species, that these hypothetical species are rapidly quenched by another reductant, or that they are unobservable by virtue of the ligation environment. An intriguing albeit speculative alternative would be a transient high-valent species formed in a side reaction pathway serving as a precursor to the tyrosyl radical. In this scenario, the tyrosyl radical might serve as a protective mechanism, whereby highly reactive intermediates that are

unavoidable due to the vagaries of the enzymatic active site, and the reaction requirements in a cellular context (at least at this point in evolutionary history) are quenched to form a more stable form that would be more easily regenerated than the product of random oxidation or hydrogen abstraction. The precise mechanistic rationalization of the OxDC tyrosyl radical identified here and its catalytic connection with the divalent metal centers of this fascinating enzyme await further study.

Acknowledgments—We thank Drs. Russell Poyner and George Reed for generating the resolution-enhanced spectra and for helpful discussion, Ixion Biotechnology for hosting C. H. C. in the early stages of the project, Dr. Ammon B. Peck for funding (NIH DK53556), and Drs. Arthur Schweiger and Ines Garcia-Rubio for helpful discussions during the sabbatical stay of A. A.

REFERENCES

1. Tanner, A., and Bornemann, S. (2000) *J. Bacteriol.* **182,** 5271–5273
2. Tanner, A., Bowater, L., Fairhurst, S. A., and Bornemann, S. (2001) *J. Biol. Chem.* **276,** 43627–43634
3. Anand, R., Dorrestein, P. C., Kinsland, C., Begley, T. P., and Ealick, S. E. (2002) *Biochemistry* **41,** 7659–7669
4. Reinhardt, L. A., Svedruzic, D., Chang, C. H., Cleland, W. W., and Richards, N. G. J. (2003) *J. Am. Chem. Soc.* **125,** 1244–1252
5. Dunwell, J. M. (1998) *Biotechnol. Genet. Engin. Rev.* **15,** 1–32
6. Stallings, W. C., Pattridge, K. A., Strong, R. K., and Ludwig, M. L. (1985) *J. Biol. Chem.* **260,** 16424–16432
7. Kolbe, H. (1849) *Ann. Chem.* **69,** 257–294
8. Vijh, A. K., and Conway, B. E. (1967) *Chem. Rev.* **67,** 623–644
9. Borodine, A. (1861) *Ann. Chem.* **119,** 121–123
10. Hunsdiecker, H., and Hunsdiecker, C. (1942) *Chem. Ber.* **75,** 291–297
11. Johnson, R. G., and Ingham, R. K. (1956) *Chem. Rev.* **56,** 219–269
12. Lowry, O. H., Rosebrough, N. J., Farr, A. L., and Randall, R. J. (1951) *J. Biol. Chem.* **193,** 265–275
13. Kim, H. W., Perez, J. A., Ferguson, S. J., and Campbell, I. D. (1990) *FEBS Lett.* **272,** 34–36
14. Glasoe, P. K., and Long, F. A. (1960) *J. Phys. Chem.* **64,** 188–190
15. Stoll, S. (2003) *Spectral Simulations in Solid-state EPR*. Ph.D. thesis, Eidgenössische Technische Hochschule, Zürich
16. Mendes, P. (1993) *Comput. Appl. Biosci.* **9,** 563–571
17. Mendes, P. (1997) *Trends Biochem. Sci.* **22,** 361–363
18. Mendes, P., and Kell, D. B. (1998) *Bioinformatics* **14,** 869–883
19. Reed, G. H., and Ballinger, M. D. (1995) *Methods Enzymol.* **258,** 362–379
20. Rupp, M., Rao, K. K., Hall, D. O., and Cammack, R. (1978) *Biochim. Biophys. Acta* **537,** 255–269
21. Padmakumar, R., and Banerjee, R. (1995) *J. Biol. Chem.* **270,** 9295–9300
22. van der Donk, W. A., Yu, G., Pérez, L., Sanchez, R. J., Stubbe, J., Samano, V., and Robins, M. J. (1998) *Biochemistry* **37,** 6419–6426
23. Whiting, A. K., Boldt, Y. R., Hendrich, M. P., Wackett, L. P., and Que, L. J. (1996) *Biochemistry* **35,** 160–170
24. Abragam, A., and Bleaney, B. (1970) *Electron Paramagnetic Resonance of Transition Metal Ions*, pp. 454 and 518, Clarendon Press, Oxford
25. Reed, G. H., and Markham, G. D. (1984) in *Biological Magnetic Resonance* (Berliner, L. J., and Reuben, J., eds) Vol. 6, pp. 73–142, Plenum Press, New York
26. Morrissey, S. R., Horton, T. E., and DeRose, V. J. (2000) *J. Am. Chem. Soc.* **122,** 3473–3481
27. Vogt, M., and DeRose, V. J. (2003) in *Paramagnetic Resonance of Metallobiomolecules* (Telser, J., ed) Vol. 858, pp. 193–211, Oxford University Press, Washington, D. C.
28. Campbell, K. A., Lashley, M. R., Wyatt, J. K., Nantz, M. H., and Britt, R. D. (2001) *J. Am. Chem. Soc.* **123,** 5710–5719
29. Krzystek, J., Yeagle, G. J., Park, J.-H., Britt, R. D., Meisel, M. W., Brunel, L.-C., and Telser, J. (2003) *Inorg. Chem.* **42,** 4610–4618
30. Campbell, K. A., Yikilmaz, E., Grant, C. V., Gregor, W., Miller, A.-F., and Britt, R. D. (1999) *J. Am. Chem. Soc.* **121,** 4714–4715
31. Rogers, P. A., and Ding, H. (2001) *J. Biol. Chem.* **276,** 30980–30986
32. Weil, J. A., Bolton, J. R., and Wertz, J. E. (1994) *Electron Paramagnetic Resonance: Elementary Theory and Practical Applications*, pp. 321–323, Wiley-Interscience, New York
33. Tommos, C., Tang, X.-S., Warncke, K., Hoganson, C. W., Styring, S., McCracken, J., Diner, B. A., and Babcock, G. T. (1995) *J. Am. Chem. Soc.* **117,** 10325–10335
34. Whittaker, M. M., and Whittaker, J. W. (2002) *J. Biol. Inorg. Chem.* **7,** 136–145
35. Kessissoglou, D. P., Li, X., Butler, W. M., and Pecoraro, V. L. (1987) *Inorg. Chem.* **26,** 2487–2492
36. Chandra, S. K., Basu, P., Ray, D., Pal, S., and Chakravorty, A. (1990) *Inorg. Chem.* **29,** 2423–2428
37. Adam, W., Mock-Knoblauch, C., Saha-Moller, C. R., and Herderich, M. (2000) *J. Am. Chem. Soc.* **122,** 9685–9691
38. Weyhermuller, T., Paine, T. K., Bothe, E., Bill, E., and Chaudhuri, P. (2002) *Inorg. Chim. Acta* **337,** 344–356
39. Rajendiran, T. M., Kampf, J. W., and Pecoraro, V. L. (2002) *Inorg. Chim. Acta* **339,** 497–502
40. Lide, D. R. *CRC Handbook of Chemistry and Physics* (1998–1999) 79th Ed., pp. (5–85)-(85–88), CRC Press, Boca Raton, FL
41. Yanez, J., Sevilla, C. L., Becker, D., and Sevilla, M. D. (1987) *J. Phys. Chem.* **91,** 487–491
42. Svistunenko, D. (2001) *Biochim. Biophys. Acta* **1546,** 365–378
43. Wagner, A. F. V., Frey, M., Neugebauer, F. A., Schäfer, W., and Knappe, J. (1992) *Proc. Natl. Acad. Sci. U. S. A.* **89,** 996–1000
44. Lassmann, G., Kolberg, M., Bleifuss, G., Gräslund, A., SJöberg, B.-M., and Lubitz, W. (2003) *Phys. Chem. Chem. Phys.* **5,** 2442–2453
45. Lendzian, F., Sahlin, M., MacMillan, F., Bittl, R., Fiege, R., Pötsch, S., Sjöberg, B.-M., Gräslund, A., Lubitz, W., and Lassmann, G. (1996) *J. Am. Chem. Soc.* **118,** 8111–8120
46. Katterle, B., Sahlin, M., Schmidt, P. P., Pötsch, S., Logan, D. T., Gräslund, A., and Sjöberg, B.-M. (1997) *J. Biol. Chem.* **272,** 10414–10421
47. Reddy, S. G., Wong, K. K., Parast, C. V., Peisach, J., Magliozzo, R. S., and Kozarich, J. W. (1998) *Biochemistry* **37,** 558–563
48. Adrait, A., Öhrström, M., Barra, A.-L., Thelander, L., and Gräslund, A. (2002) *Biochemistry* **41,** 6510–6516
49. Stubbe, J., and van der Donk, W. A. (1998) *Chem. Rev.* **98,** 705–762
50. Ehrenberg, A., and Reichard, P. (1972) *J. Biol. Chem.* **247,** 3485–3488
51. Tsai, A.-L., and Kulmacz, R. J. (2000) *Prostag. Others Lipid M.* **62,** 231–254
52. Barry, B. A., El-Deeb, M. K., Sandusky, P. O., and Babcock, G. T. (1990) *J. Biol. Chem.* **265,** 20139–20143
53. Gerfen, G. J., van der Donk, W. A., Yu, G., McCarthy, J. R., Jarvi, E. T., Matthews, D. P., Farrar, C., Griffin, R. G., and Stubbe, J. (1998) *J. Am. Chem. Soc.* **120,** 3823–3835
54. Chen-Barrett, Y., Harrison, P. M., Treffry, A., Quail, M. A., Arosio, P., Santambrogio, P., and Chasteen, N. D. (1995) *Biochemistry* **34,** 7847–7853
55. Stubbe, J., Nocera, D. G., Yee, C. S., and Chang, M. C. Y. (2003) *Chem. Rev.* **103,** 2167–2201
56. Sun, X., Ollagnier, S., Schmidt, P. P., Atta, M., Mulliez, E., Lepape, L., Eliasson, R., Gräslund, A., Fontecave, M., Reichard, P., and Sjöberg, B.-M. (1996) *J. Biol. Chem.* **271,** 6827–6831
57. Parast, C. V., Wong, K. K., and Kozarich, J. W. (1995) *Biochemistry* **34,** 5712–5717
58. van der Donk, W. A., Stubbe, J., Gerfen, G. J., Bellew, B. F., and Griffin, R. G. (1995) *J. Am. Chem. Soc.* **117,** 8908–8916